Ecological Modelling 477 (2023) 110271

Contents lists available at ScienceDirect

Ecological Modelling

journal homepage: www.elsevier.com/locate/ecolmodel

Implications of seasonal changes in photosynthetic traits and leaf area index for canopy CO_2 and H_2O fluxes in a Japanese cedar (*Cryptomeria japonica* D. Don) plantation

Yoshiaki Hata [a,*], Tomo'omi Kumagai [a,b,c], Takanori Shimizu [d], Yoshiyuki Miyazawa [e]

[a] Graduate School of Agricultural and Life Sciences, The University of Tokyo, Bunkyo-ku, Tokyo 113-8657, Japan
[b] Institute for Space-Earth Environmental Research, Nagoya University, Chikusa-ku, Nagoya 464-8601, Japan
[c] Water Resources Research Center, University of Hawai'i at Mānoa, Honolulu, HI 96822, USA
[d] Forestry and Forest Products Research Institute, Tsukuba, Ibaraki 305-8687, Japan
[e] Office for Campus Planning, Kyushu University, Motooka, Fukuoka 819-0395, Japan

ARTICLE INFO

Keywords:
Eddy covariance
Soil–vegetation–atmosphere transfer model
Canopy photosynthesis
Canopy transpiration
Leaf area index
Net ecosystem carbon exchange

ABSTRACT

Recently, requests for forest management to conserve water resources and sequester carbon have increased in Japan, where approximately 27% and 12% of the total land area are covered by forest plantations and Japanese cedar (*Cryptomeria japonica* D. Don). To formulate better forest management practices that maximize forest functions by maintaining water and carbon cycles, an understanding of how leaf-level ecophysiological traits influence canopy-level CO_2 and H_2O exchanges in Japanese cedar plantations is required. In this study, observations of eddy covariance flux and leaf ecophysiology in a Japanese cedar plantation in southern Japan indicate that significantly greater productivity and seasonal variations tend to occur in canopy CO_2 and H_2O fluxes, with seasonal patterns of photosynthetic traits (maximum carboxylation rate normalized at 25 °C, $V_{cmax,25}$) and leaf area index (LAI). We also examined how biotic (e.g., $V_{cmax,25}$ and LAI) and abiotic (e.g., meteorological variables) factors govern canopy fluxes using a multi-layer soil–vegetation–atmosphere transfer (SVAT) model. The model validation suggests that seasonal variations in $V_{cmax,25}$ and LAI must be included to reproduce the fluxes observed in the plantation. Quantitative experiments using the validated SVAT model indicate that considering cold acclimation during the winter improved the reproducibility of the model with regard to the measured fluxes, constant high intra-annual LAI had the least impact on forest productivity, and a consistently high $V_{cmax,25}$ value increased forest productivity but considerably decreased the nitrogen use efficiency and required a larger nitrogen supply from the ecosystem during the winter. These findings highlight the necessity of decreasing photosynthetic ability during the winter, which safeguards the ecosystem's nitrogen resources to sustain the productivity of the Japanese cedar plantation throughout the year.

1. Introduction

Forests cover ~70% of the total land area in Japan, and are mostly located in mountainous regions. Forest plantations and forests that contain a single conifer species (Japanese cedar, *Cryptomeria japonica* D. Don) cover approximately 27% and 12% of the total land area, respectively (Japan Forestry Agency, 2021). Thus, Japanese forest plantations that are mainly composed of evergreen conifers such as Japanese cedar play a substantial role in supplying water resources to lowlands (e.g., Momiyama et al., 2021) and sequestering large amounts of carbon from the atmosphere. Egusa et al. (2020) estimated that at least 40 Tg year^{-1} of net carbon was taken up by Japanese forests, of which the presumed contribution of Japanese cedar is approximately one-fourth of the total uptake. Recently, requests for forest plantation management to control water discharge from the mountains and maximize carbon sequestration have increased (Japan Forestry Agency, 2021). In addition, to mitigate the negative impacts of climate change and land use on the anticipated forest functions, an improved understanding of the carbon and water cycle processes in Japanese cedar plantations is required, which can provide strategies for forest plantation management.

Few studies have assessed canopy-level CO_2 and H_2O exchanges in Japanese cedar plantations by the eddy covariance method, which is a

* Corresponding author.
E-mail address: yoshiakihata0806@gmail.com (Y. Hata).

https://doi.org/10.1016/j.ecolmodel.2022.110271
Received 5 June 2022; Received in revised form 1 December 2022; Accepted 29 December 2022

prerequisite for assessing forest carbon and water cycle processes (Saitoh et al., 2010; Shimizu et al., 2015). Previous studies have focused on the importance of Japanese cedar as a woody material and as a silvicultural species (e.g., Ohsumi, 2018). Further, few studies have examined the leaf-scale ecophysiology of Japanese cedar, which is critical for understanding the mechanisms of canopy CO_2 and H_2O exchanges (e.g., Han et al., 2003; Miyazawa et al., 2017). The ability to understand existing carbon and water cycling and predict future cycling under a changing environment in Japanese cedar plantations has been limited, owing to the lack of integrated leaf- and canopy-scale data for model input and evaluation.

Numerous simple big-leaf canopy frameworks have been used to describe CO_2 and H_2O fluxes from the canopy by coupling ecophysiological principles with above-canopy aerodynamic transport mechanics, which have also been adopted in land surface models (e.g., Lawrence et al., 2019; Sellers et al., 1996). However, Bonan et al. (2021) noted the limitations of a big-leaf scheme, which are caused by ignoring vertical microclimate profiles and leaf physiology in the canopy, and suggested the necessity of using a multi-layer formulation for the canopies to achieve a thorough understanding of the fluxes (e.g., Baldocchi and Meyers, 1998; Katul and Albertson, 1999; Lai et al., 2000). In this study, a multi-layer soil–vegetation–atmosphere transfer (SVAT) model was parameterized using independently collected leaf-level ecophysiological measurements and was not calibrated or parameterized using canopy-level flux measurements (e.g., Kumagai and Kume, 2012; Kumagai et al., 2006, 2013; Xue et al., 2011). The SVAT model used herein is useful for investigating the effects of meteorological factors and/or ecophysiological functions on CO_2 and H_2O exchanges between the forest canopy and the atmosphere.

Although seasonal variations in photosynthetic traits have been considered in SVAT models to accurately estimate CO_2 and H_2O fluxes (e.g., Wilson et al., 2001), little attention has been paid to flux simulations in evergreen conifer biomes (e.g., Wang et al., 2019). Moreover, evergreen conifers are known to exhibit seasonal photosynthetic traits, despite their constant greenness (e.g., Bourdeau, 1959). Recent studies have demonstrated the mechanism by which evergreen conifer trees regulate seasonal photosynthetic activity (e.g., Bowling et al., 2018; Yang et al., 2020). Bowling et al. (2018) and Seyednasrollah et al. (2021) examined the relationships between gross primary productivity (GPP) and canopy color associated with leaf pigment to predict seasonal variations in GPP for evergreen conifer forests. Luo et al. (2019) reported that the simulated GPP of evergreen conifers was less accurate after applying the seasonal leaf chlorophyll content constraint, considering the seasonal variations in photosynthetic traits. Wang et al. (2019) found that the big-leaf scheme in a land surface model could better reproduce eddy covariance-measured daily GPP and evapotranspiration values for evergreen conifer forests when considering seasonal variations in photosynthetic traits and leaf area index (LAI). However, seasonal variations in photosynthetic traits have rarely been used to constrain land surface models for evergreen conifers; thus, the observation of seasonal variations in photosynthetic traits, LAI of evergreen conifers, and their application to multi-layer SVAT models should be investigated both locally and globally.

The primary objective of this study was to investigate how seasonally varying leaf ecophysiology and meteorological factors affect the canopy CO_2 and H_2O fluxes in a Japanese cedar plantation. The colors of the cedar canopy differ between the winter and the growing season, resulting in a higher photosynthetic ability during the growing season (e.g., Han and Mukai, 1999). In this study, we addressed three main questions: (1) To what degree do photosynthetic traits and LAI vary seasonally? (2) How large of an impact does seasonality in photosynthetic traits and LAI have on canopy flux processes? (3) The ecological implications of deciduous behavior are generally related to meteorological seasonality; hence, what ecological implications underlie seasonal variations in photosynthetic traits and LAI in evergreen conifers? To address these questions, we collected detailed field measurements of leaf-scale gas exchange, LAI, and eddy covariance fluxes. Using these data, we analyzed the factors controlling canopy fluxes with a multi-layer SVAT model. Prior to assessing the impacts of the seasonality of photosynthetic traits and LAI on the canopy fluxes, the SVAT model was validated using field measurements collected during one year in a Japanese cedar plantation in Kyushu, Japan.

2. Study site and observations

The study site and instruments relevant to the meteorological and flux measurements are described in Kumagai et al. (2014) and Shimizu et al. (2015). A review, the leaf-level ecophysiology measurements, and leaf area density profile measurements are provided here for clarity.

2.1. Site description

Experiments were carried out in a 2.63 ha sub-catchment in the Kahoku Experimental Watershed (KHEW) on the island of Kyushu, Japan (33°08′ N, 130°43′ E, 150–220 m a.s.l.). This sub-catchment is underlain by crystalline schist and the slopes on both sides of the valley are steep (20–40°). The mean annual precipitation in the study area during 2000–2008 was 2183 mm, with a rainy season that occurs from mid-June to early July. The mean annual temperature during 2000–2008 was 15.3 °C, with a minimum mean monthly temperature of ~4 °C during January–February and a maximum mean monthly temperature of ~26 °C during August.

Forests in this sub-catchment mainly consist of 52-year-old (as of 2007) Japanese cedar stands. Japanese cypress (*Chamaecyparis obtuse* Endl.) stands are also present in the study area, ranging in age from 30 to 52 years (as of 2007). Japanese cedar trees are dominant on the right stream bank, whereas Japanese cypress and broadleaved tree species cover the left stream bank and compete with the planted conifers (see Fig. 1 in Shimizu et al., 2015). The understory vegetation comprises various evergreen tree species, including *Quercus glauca* Thunb., *Castanopsis sieboldii* Hatsusima ex Yamazaki et Mashiba, and *Eurya japonica* Thunb.

2.2. Meteorological and flux measurements

We measured meteorological factors and eddy covariance fluxes using a 52 m over-canopy tower at the center of the sub-catchment. An albedo meter (CM14B, Kipp & Zonen, Delft, Netherlands) and two pyrgeometers (CG3, Kipp & Zonen) were installed at a height of 47.2 m to measure the upward shortwave radiation, incident solar radiation (R_s), and upward and downward infrared radiation, respectively. The net radiation (R_n) was calculated as the total of these four radiation values. Air temperature (T_a) and relative humidity were measured using two ventilated psychrometers (MH-020L, EKO Instruments, Tokyo, Japan) installed at heights of 42.0 m and 20.0 m, respectively. Precipitation (P) was measured using a tipping bucket rain gauge (RT-5, Ikeda Keiki, Tokyo, Japan) placed on a waist-high bench in an open field approximately 100 m from the watershed. Discharge (Q) from the sub-catchment was also recorded using a weir and float-level meter (ADR-115D, Ikeda Keiki). The wetness index (WI; Shimizu et al., 2015) in the watershed was defined as $WI = \min\{(Q_R/Q_{max90})^{0.2}, 1\}$, where Q_R is the representative Q measured in another sub-catchment in the watershed and Q_{max90} is the maximum Q_R during the past 90 days. Note that WI was only used for quality control (QC) for the eddy covariance fluxes (see Supplementary material).

Soil heat flux (G) and temperature (T_{5cm}) at a depth of 5 cm were measured near the tower using a heat flux plate (HFT3.1, REBS, Seattle, WA, USA) and a thermistor (TR-71U, T&D Corp., Nagano, Japan) that was waterproofed with a polyethylene tube and silicone. The volumetric soil moisture contents (θ) at 10, 20, and 40 cm beneath the forest floor were measured using dielectric aquameter sensors (EC-10, Decagon Devices, Inc., Pullman, WA, USA). A weighted average of θ in the 0–50

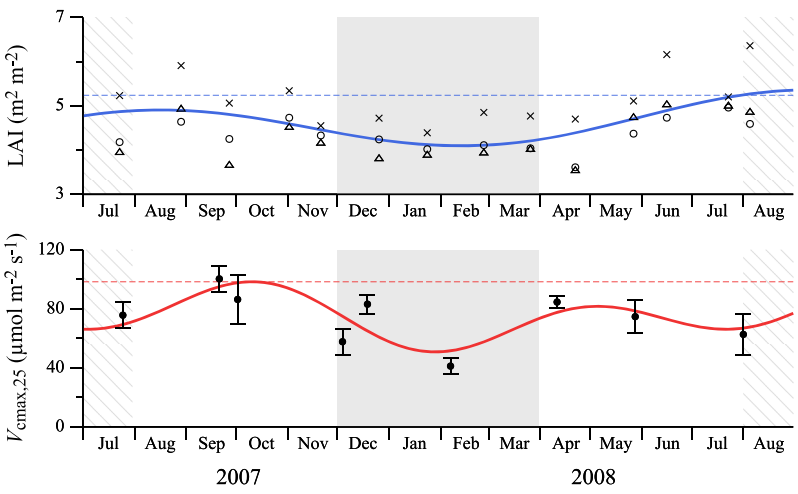

Fig. 1. Seasonal variations in (a) the total leaf area index (LAI), including the understory vegetation, at three observation points (the same symbols denote the same observation points) and (b) the projected shoot area-based maximum carboxylation rate normalized at 25 °C ($V_{cmax,25}$) with ±1 standard errors (i.e., vertical bars) at the top of the cedar canopy. Solid and horizontal dashed lines represent the approximate curves and the estimated maximum values, respectively. The hatched and shaded zones represent the non-simulated and winter periods, respectively.

cm soil layer ($\theta_{0–50}$) was calculated as $\theta_{0–50} = (15\theta_{10} + 15\theta_{20} + 20\theta_{40})/50$, where θ_{10}, θ_{20}, and θ_{40} are the θ values at depths of 10, 20, and 40 cm, respectively.

Three-dimensional wind speed (u) and gas (CO_2 and H_2O) concentration time series data were collected at a height of 51.0 m with a 10 Hz sampling frequency using a three-dimensional sonic anemothermometer (SAT: DA-600-3T/TR-61C, Kaijo, Tokyo, Japan) co-located with a gas-inlet that led to a closed-path infrared gas analyzer (IRGA: LI-7000, Li-Cor, Lincoln, NE, USA). All variances and covariances required for the eddy-covariance flux estimates were computed using a 30-min average interval. Air samples were obtained using gas inlets at 6.0, 11.5, 17.3, 24.0, 31.2, 36.5, 40.3, and 46.1 m above ground level, and CO_2 concentrations were measured using an IRGA (LI-6262, Li-Cor). The net ecosystem CO_2 exchange (NEE) was obtained as the sum of the above-canopy CO_2 flux (F_c), which was obtained using the eddy covariance system above the canopy, and the within-canopy storage flux (S_c), which was determined by quantifying the rate of change of the CO_2 concentration in the air column within the canopy (i.e., NEE = $F_c + S_c$). The QC for the processed flux data was described in the Supplementary material.

In this study, flux data within 48 h after a rainfall event were discarded, thereby allowing us to understand the canopy transpiration rate (E) from the dry canopy. To validate the proposed SVAT model, the flux data when $R_s > 350$ W m^{-2} and $u < 0.1$ m s^{-1}, or when $R_s > 500$ W m^{-2} and $u < 1.0$ m s^{-1} were discarded, as the model output unreasonably high leaf and soil surface temperatures under low u and high incident radiation conditions.

The CO_2 efflux from the soil surface was measured during other observational campaigns at the study site (Ishizuka et al., 2006; Tamai, 2010). The soil CO_2 efflux data were averaged over the measurement points, which was regarded as the half-hourly value of soil respiration (R_{soil}, μmol m^{-2} s^{-1}). In the SVAT model used herein, R_{soil} was expressed as a power function given by the following equation:

$$R_{soil} = R_{soil,0} Q_{10}^{\frac{T_{soil}-273.15}{10}} \quad (1)$$

where $R_{soil,0}$ and Q_{10} are the fitted parameters representing R_{soil} at 0 °C and the rate of increase when soil surface temperature (T_{soil}) increased by 10 °C, respectively. Parameters $R_{soil,0}$ and Q_{10} were estimated to be 0.135 μmol m^{-2} s^{-1} and 3.63, respectively (Table 1), using least-squares regression analysis ($R^2 = 0.91$) (Ishizuka et al., 2006). To avoid overestimating R_{soil} when T_{soil} was high, we set the upper limit of R_{soil} as 4.03 μmol m^{-2} s^{-1}, according to observations made by Tamai (2010).

Table 1
Major parameters used for the SVAT model validation. Values in parentheses represent parameters used for understory vegetation.

Parameter[a]	Value	Units
Total LAI[b]	4.1–5.2 (1.3–1.6)	m^2 m^{-2}
Canopy height	32.0 (10.4)	m
Ω(0)	0.6 (0.9)	unitless
$V_{cmax,25}$	50.8–98.4 at the *Cr. japonica* canopy top [c] (33.0)	μmol m^{-2} s^{-1}
$J_{max,25}$	$1.63V_{cmax,25}$ ($1.70V_{cmax,25}$)	μmol m^{-2} s^{-1}
$R_{d,25}$	$0.056V_{cmax,25}$ ($0.033V_{cmax,25}$)	μmol m^{-2} s^{-1}
k_n[d]	0.47, 0.92, 0.85 (0.29)	unitless
g_1	4.65 (3.40)	kPa$^{0.5}$
$R_{soil,0}$	0.135	μmol m^{-2} s^{-1}
Q_{10}	3.63	unitless

[a] Ω(0) is the clumping factor when looking up out of the canopy toward the zenith; $V_{cmax,25}$ indicates the maximum carboxylation rate normalized at 25 °C; $J_{max,25}$ represents the potential rate of whole-chain electron transport at 25 °C; $R_{d,25}$ denotes the dark respiration rate at 25 °C; k_n is the nitrogen distribution attenuation coefficient; g_1 is the slope parameter for stomatal conductance model; $R_{soil,0}$ represents the soil surface CO_2 efflux at 0 °C; Q_{10} is the increase rate of soil surface CO_2 efflux when soil surface temperature increases by 10 °C.
[b] See Fig. 1a.
[c] See Fig. 1b.
[d] Values for winter, growth period, and the entire study period.

2.3. Leaf area and leaf-level ecophysiology measurements

Total LAI, including understory vegetation, was measured every month during the study period at three LAI observation points in the sub-catchment using a plant canopy analyzer (LAI-2000, Li-Cor) (Fig. 1a). We obtained a significantly higher LAI at one observation point ($p < 0.001$, paired t-test). Fitting an approximate second-order Fourier curve to the LAI data yielded $\mathrm{LAI}(t) = \sum_{i=0}^{2}\{a_i\cos(irt) + b_i\sin(irt)\}$, where t is time (day; $t = 1$ is July 1, 2007), $a_0 = 4.547$, $a_1 = -0.2577$, $a_2 = 0.4825$, $b_1 = 0.06826$, $b_2 = 0.3233$, and $r = 0.00776$. The LAI ranged from 4.1 to 5.2 m^2 m^{-2} and exhibited minor seasonal variations (Table 1). We defined April–November and December–March as the growth and winter periods, respectively, which corresponded to a significantly higher LAI in April–November ($p < 0.01$, t-test) (Fig. 1a).

Vertical LAI profiles within the canopy were measured at eight heights using 1–5 m intervals along three vertical observation lines, using a plant canopy analyzer, LAI-2000, on the tower. We then obtained the vertical leaf area density (a_{leaf}) profile, which was calculated as the difference in LAI between the two nearest neighboring heights divided by the interval (Fig. 2). Here, we obtained a local minimum point at 10.4 m, which was estimated as the understory vegetation

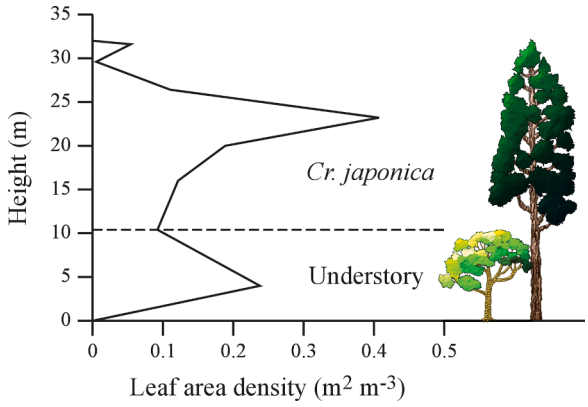

Fig. 2. Vertical distribution of leaf area density within the canopy. Heights of Japanese cedar (*Cr. japonica*) trees and understory vegetation (indicated by a horizontal dashed line) were estimated as 32.0 m and 10.4 m, respectively.

height (Table 1). We assumed that the canopy height (h_c) and LAI ratio of Japanese cedar to the understory vegetation were 32.0 m and 2.1, respectively.

Leaf-level ecophysiological traits were measured nine times from July 2007 to August 2008. Using a portable photosynthesis measurement system (LI-6400, Li-Cor), the relationship between the net photosynthetic rate (A_n) and intercellular CO_2 concentrations (C_i) (A_n–C_i curve) was obtained for the excised shoots of four Japanese cedar trees adjacent to the observation tower. Overall, 5–16 shoots (including young needle leaves and twigs) were selected for each photosynthesis measurement from the upper crowns that were exposed to the sun and within the horizontal reach of a pole pruner from the tower. Notably, we previously confirmed the negligible impact of excision on leaf gas exchange or its simulation (Miyazawa et al., 2017), following the procedure described by Miyazawa et al. (2011). We then determined the photosynthetic parameters described by Farquhar et al. (1980): the maximum ribulose bisphosphate (RuBP) carboxylation (V_{cmax}) rate at 25 °C ($V_{cmax,25}$), which was obtained for the sampled shoots by measuring light-saturated A_n under six CO_2 concentrations and by regressing A_n with C_i using the equation in Farquhar et al. (1980) on A_n limited by RuBP carboxylase-oxygenase (Rubisco) activity. In this study, the $V_{cmax,25}$ of Japanese cedar was estimated as the value per shoot-projected area. We assumed that $J_{max,25} = 1.63V_{cmax,25}$, and $R_{d,25} = 0.056V_{cmax,25}$ (where $J_{max,25}$ and $R_{d,25}$ are the potential rate of whole-chain electron transport (J_{max}) and the dark respiration rate (R_d) at 25 °C, respectively), based on measurements by Wullschleger (1993) and this study. A second-order Fourier approximate curve was fitted to the estimated $V_{cmax,25}$ data, yielding $V_{cmax,25}(t) = \sum_{i=0}^{2}\{a_i\cos(irt) + b_i\sin(irt)\}$, where t is time (days; $t = 1$ is July 1, 2007), $a_0 = 74.33$, $a_1 = 5.896$, $a_2 = -13.98$, $b_1 = 9.785$, $b_2 = -6.022$, and $r = 0.01637$ (Fig. 1b). The mean $V_{cmax,25}$ for each measurement ranged from 50.8 (February) to 98.4 μmol m^{-2} s^{-1} (September) (Table 1). The maximum $V_{cmax,25}$ during the winter was significantly smaller than during the growth period ($p < 0.01$, t-test) (Fig. 1b).

The photosynthetic traits of the understory vegetation were measured in three individuals per species, (i.e., *Q. glauca, Ca. sieboldii*, and *E. japonica*) and 8–10 current-year leaves per individual around the observation tower were sampled every two or three months during the study period. Gaseous exchange in leaves within the cuvette was measured *in-situ* using a portable photosynthesis measurement system (LI-6400) under light saturation and at 11 cuvette CO_2 concentrations to obtain the $V_{cmax,25}$ values. Although photosynthetic traits are known to change with leaf age (Escudero and Mediavilla, 2003), the area ratio of older leaves was much smaller than that of the current-year leaves in each individual; therefore, we assumed that the photosynthetic traits of all leaves were the same as those of the current-year leaves. In addition, we found that the estimated $V_{cmax,25}$ values were somewhat constant within 20–50 μmol m^{-2} s^{-1} regardless of the seasonality or species. Thus, we set the value for the understory vegetation $V_{cmax,25}$ as 33.0 μmol m^{-2} s^{-1} throughout the study period (Table 1).

3. Methodology

3.1. SVAT model description

The SVAT model (Kumagai et al., 2006, 2013) used in this study consists of three major sub-models (Fig. 3). Computational domains for the canopy and atmosphere above it were divided into 50 layers each.

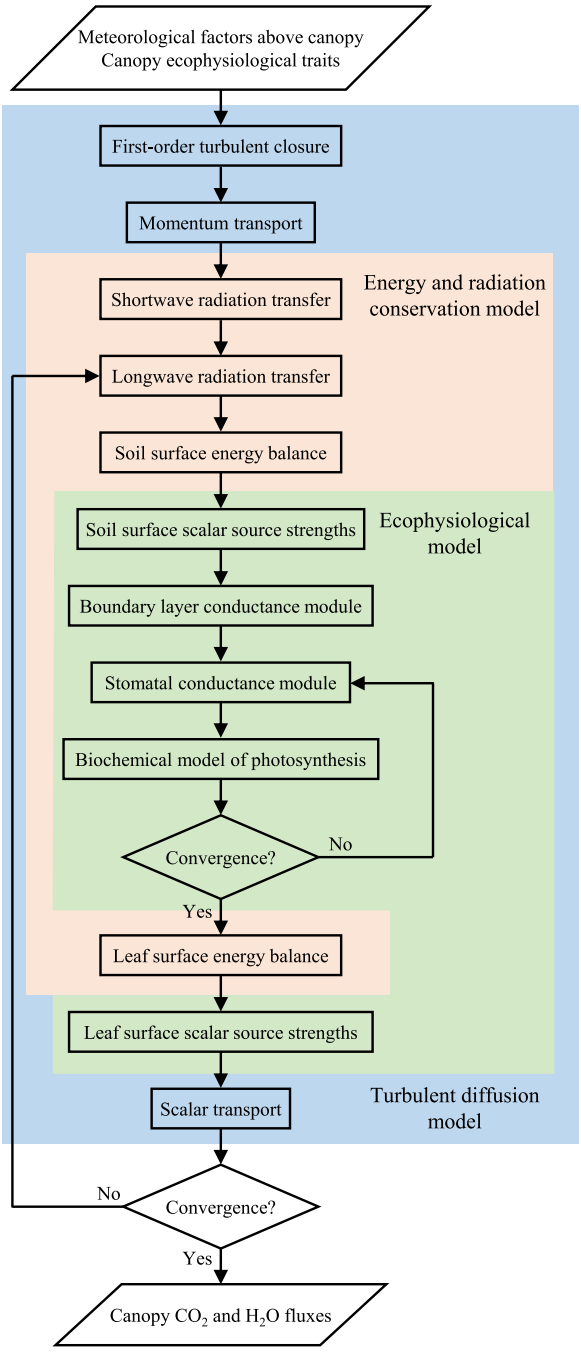

Fig. 3. Conceptual diagram of the SVAT model used in this study. The model contains three major sub-models: (1) a model for energy and radiation conservation; (2) an ecophysiological model for stomatal opening and carbon assimilation; and (3) a model for turbulent diffusion.

All of the equations in this model were solved for each layer. In the model, we updated the sub-models for stomatal conductance and daytime respiration rate. We also accounted for the clumped conifer foliage. A brief description of the modeling scenario used herein and explanations of the new components are provided in the following sub-sections (cf. Kumagai et al., 2006, 2013).

3.1.1. Radiative transfer and energy balance at leaf and soil levels

When considering the leaf-scale energy balance and photosynthesis within a forest canopy, radiative transfer through the canopy must be determined. Direct beam and diffuse irradiance must be considered separately, owing to their differing attenuations in the canopy. The probability of no contact for beam irradiance (P_b) within a canopy layer must be formulated to describe the direct irradiance transfer within the canopy. This formulation includes a_{leaf}, which is the beam extinction function of the solar elevation and leaf angle distribution within a given layer (Goudriaan, 1977).

Conifers are generally regarded as having clumped foliage, as their needle leaves are organized onto the shoots. In this study, we incorporated a clumping factor (Ω) in the P_b equation by replacing a_{leaf} with Ωa_{leaf}, where Ω is a function of the solar zenith angle (ψ) (Campbell and Norman, 1998):

$$\Omega(\psi) = \frac{\Omega(0)}{\Omega(0) + (1 - \Omega(0))\exp(-2.2\psi^{\omega})} \tag{2}$$

where $\Omega(0)$ is the clumping factor when looking up out of the canopy toward the zenith, ω is given by $3.80 - 0.46D_{crown}$, D_{crown} is the ratio of crown depth to crown diameter and is considered to be 1 or 3.34 when ω is less than 1 or greater than 3.34, respectively. The probability of no contact for diffuse irradiance (P_d) within the canopy layer was calculated by integrating P_b over the solid angles of the sky hemisphere. Downward and upward longwave radiation (R_L) transfer within the canopy followed the theories of diffuse irradiance transfer. It is noteworthy that R_L was emitted from any plant body within the canopy.

Both direct and diffuse solar radiation can be further divided into photosynthetic active radiation (PAR) and near-infrared radiation (NIR), based on their absorptions by leaves. Approximately half of the R_s over the canopy is PAR, while the other half is NIR, thereby enabling estimates of R_s penetration inside the canopy. The absorbed PAR or NIR within the canopy layer between z (height above the ground) and $z + \Delta z$, ΔS, is defined by the following equations:

$$\Delta S_b = (1 - P_b)(1 - \eta - \xi)S_b(z + \Delta z) \tag{3}$$

$$\Delta S_d^{\downarrow} = (1 - P_d)(1 - \eta - \xi)S_d^{\downarrow}(z + \Delta z) \tag{4}$$

$$\Delta S_d^{\uparrow} = (1 - P_d)(1 - \eta - \xi)S_d^{\uparrow}(z) \tag{5}$$

where η and ξ are the leaf transmissivity and reflectivity, respectively, for PAR or NIR and S is the PAR or NIR at a given height. Subscripts "b" and "d" denote direct beam and diffuse irradiation, respectively, and the superscript arrows denote the irradiation direction. Note that Eqs. (3)–(5) are not simple 2-stream radiative transfer models, as P_b and P_d are complex functions of a_{leaf}, leaf angle distribution, and Ω within a given canopy layer and for a given solar geometric direction Kumagai et al., 2006). The total absorbed solar radiation within the canopy layer was then calculated as the sum of the absorbed PAR and NIR, which were calculated using Eqs. (3)–((5). Sunlit leaves receive the beam, as well as upward and downward diffuse radiation, whereas shaded leaves only receive upward and downward diffuse radiation. Therefore, irradiance absorption and energy balance must be computed separately for sunlit and shaded leaves (Kumagai et al., 2006).

The energy balance at the soil surface used to compute T_{soil}, is expressed using the following equation:

$$R_{sab\_soil} + R_{L\_down}(0) - \varepsilon_s \sigma T_{soil}^4 = H_{soil} + LE_{soil} + G \tag{6}$$

where R_{sab_soil} is the total R_s absorbed by the soil surface, $R_{L\_down}(0)$ is the downward R_L at $z = 0$, ε_s is the soil emissivity, σ is the Stefan-Boltzmann constant (5.67×10^{-8} W m^{-2} K^{-4}), and H_{soil} and LE_{soil} are the sensible and latent heat fluxes at the soil surface, respectively. H_{soil} and LE_{soil} are functions of T_{soil}, as described by the products of transport conductance and concentration difference. In addition, the soil surface moisture availability was used to compute LE_{soil} (Kumagai et al., 2006). G is a sinusoidal function of time (Kumagai et al., 2013).

3.1.2. Leaf-level ecophysiological functions

The leaf-level scalar source strengths, i.e., leaf sensible heat flux (H_l), transpiration rate (E_l), and net photosynthesis rate (A_l), can be obtained from physiological controls using the following equations:

$$H_l = 2m_a c_p g_{ah}(T_l - T_a) \tag{7}$$

$$E_l = m_w \frac{g_{aw} g_{sw}}{g_{aw} + g_{sw}} \frac{e_{sat}(T_l) - e}{p_a} \tag{8}$$

$$A_l = g_{ac}(C_a - C_s) \tag{9}$$

$$A_l = g_{sc}(C_s - C_i) \tag{10}$$

where m_a and m_w are the molecular weights of air and water, respectively; c_p is the specific heat of air at a constant pressure; $e_{sat}(T_l)$ and e are the saturated vapor pressure at the leaf temperature (T_l) and atmospheric vapor pressure, respectively; p_a is the atmospheric pressure; and C_s, C_a, and C_i are the CO_2 concentrations of the air inside and outside the laminar boundary layer of the leaves and within the stomatal cavity, respectively. g_{ah}, g_{aw}, and g_{ac} are the boundary layer conductances of heat, water vapor, and CO_2, respectively, calculated according to the methods described by Campbell and Norman (1998). g_{sw} and g_{sc} are the stomatal conductances for water vapor and CO_2, respectively. g_{sw} is linked to A_l, C_a, and the vapor pressure deficit at the leaf surface (D_l), as proposed by Medlyn et al. (2011) in the following equation:

$$g_{sw} = g_0 + 1.6\left(1 + \frac{g_1}{\sqrt{D_l}}\right)\frac{A_l}{C_a} \tag{11}$$

where g_0 and g_1 are the parameters representing positive nighttime conductance and a value proportional to $\sqrt{\Gamma^* \lambda}$ (where Γ^* is the CO_2 compensation point and λ is the marginal water cost of carbon gain), respectively. g_0 and g_1 were assumed to be 0.01 mol m^{-2} s^{-1} and 4.60 kPa$^{0.5}$ (Table 1) (Lin et al., 2015; Miner et al., 2017). g_{sc} was obtained from $g_{sc} = g_{sw}/1.6$, where 1.6 is the ratio of the diffusivities of water and CO_2 in air (von Caemmerer and Farquhar, 1981).

A_l was computed using the biochemical model of Farquhar et al. (1980) and Collatz et al. (1991) as a minimum value of the gross rate of photosynthesis limited by Rubisco activity (A_v), the rate of RuBP regeneration through electron transport (A_j), and the export rate of synthesized sucrose (A_s), as illustrated by the following equation:

$$A_l = \min(A_v\ ,\ A_j\ ,\ A_s) - R_l \tag{12}$$

where R_l is the respiration rate during the day and nighttime in the absence of photosynthesis. R_d is suppressed in light compared to a dark scenario due to the Kok effect (Heskel et al., 2013; Yin et al., 2020). Thus, the R_l in the SVAT model is given by the following equation (Wohlfahrt et al., 2005):

$$R_l = R_d\left\{1 - \frac{(1 - a_{Kok})Q_P}{b_{Kok} + Q_P}\right\} \tag{13}$$

where a_{Kok} and b_{Kok} are parameters (set as 0.5 and 2.0 μmol m^{-2} s^{-1}, respectively), and Q_P (μmol m^{-2} s^{-1}) is the absorbed PAR per leaf area. The formulation and parameterizations of A_v, A_j, A_s, and R_d as functions of Q_P, C_i, and T_l were used (Collatz et al., 1991; de Pury and Farquhar, 1997; Farquhar and Wong, 1984; Farquhar et al., 1980; Kumarathunge

et al., 2019). The photosynthetic model constants were determined according to the findings of previous studies (e.g., Badger and Collatz, 1977; Bernacchi et al., 2001, 2003; de Pury and Farquhar, 1997; Farquhar et al., 1980; von Caemmerer et al., 1994). The V_{cmax} and J_{max} values used in these calculations are expressed as non-linear functions of temperature using $V_{cmax,25}$ and $J_{max,25}$, respectively, the formulations of which were described by de Pury and Farquhar (1997). R_d is expressed as a nonlinear function of temperature using $R_{d,25}$. Both $J_{max,25}$ and $R_{d,25}$ are practically related to $V_{cmax,25}$, and $V_{cmax,25}$ is the key parameter in the leaf photosynthesis model.

3.1.3. Momentum and scalar transport

The momentum, scalar continuity, and turbulent flux equations were obtained by assuming a steady-state planar-homogeneous state. The turbulent Schmidt number for a scalar is unity, and a first-order turbulent closure scheme was applied using time and horizontal averaging, as shown in the following equation:

$$0 = \frac{\partial}{\partial z}\left(K_t \frac{\partial \varphi}{\partial z}\right) + S_\varphi \tag{14}$$

where K_t is the eddy turbulent diffusivity, φ is a variable such as wind speed (U), air temperature (T), specific humidity (q), and air CO_2 concentration (C). S_φ is a source (or sink) term for φ because of the drag force and mass release (or uptake) by the ensemble of leaves within the averaging plane, which is given by the following equations:

$$S_U = -\, c_d a_{leaf} U^2 \tag{15}$$

$$S_T = \frac{1}{\widehat{\rho} c_p}\left(H_{l\_sl} a_{leaf\_sl} + H_{l\_sh} a_{leaf\_sh}\right) \tag{16}$$

$$S_q = \frac{1}{\widehat{\rho}}\left(E_{l\_sl} a_{leaf\_sl} + E_{l\_sh} a_{leaf\_sh}\right) \tag{17}$$

$$S_C = -\left(A_{l\_sl} a_{leaf\_sl} + A_{l\_sh} a_{leaf\_sh}\right) \tag{18}$$

where c_d is the drag coefficient (0.06) and $\widehat{\rho}$ is the air density. To calculate K_t, we used the mixing length theory of Kondo and Watanabe (1992). The subscripts "sl" and "sh" refer to sunlit and shaded leaves, respectively. In general, first-order closure principles are applicable when the production term is balanced by the dissipation term in a scalar flux budget with minimal contributions from gradients in the turbulent flux transport terms, which is generally satisfied in the forest canopy studied here (Manzoni et al., 2011).

3.2. Model computation

The SVAT model used in this study was parameterized using independently collected values from ecophysiological measurements or references, and was not calibrated or parameterized using canopy-level flux measurements. After model validation using the canopy flux measurements, the model could examine how seasonal patterns of $V_{cmax,25}$ and LAI (Fig. 1) are generated, thereby determining the way in which ecophysiological traits control NEE and E in the Japanese cedar plantation in this study. Thus, we conducted four types of model simulation, as listed in Table 2.

Variability in $V_{cmax,25}$ due to vertical gradients in the light environment is described by changes in leaf nitrogen per unit area (Niinements and Tenhunen, 1997). Thus, in accordance with Leuning et al. (1995), we assumed that $V_{cmax,25}$ at canopy position z can be expressed as decreasing exponentially with cumulative LAI ($\xi(z)$) from h_c to z, as in the following equation:

$$V_{cmax,25}(z) = V_{cmax,25}(h_c)\exp(-k_n \xi(z)) \tag{19}$$

where k_n is the attenuation coefficient, which is the only calibration parameter used in the SVAT model. It should be noted that $V_{cmax,25}(h_c)$ denotes the measured $V_{cmax,25}$ at h_c and the temporal variations in $V_{cmax,25}(z)$ are assumed to be expressed by variations in $V_{cmax,25}(h_c)$. In addition, temporal variations in a_{leaf} at z were expressed using the following equation:

$$a_{leaf}(z) = \frac{LAI}{\int_0^{h_c} a_{leaf\_o}(z)dz} a_{leaf\_o}(z) \tag{20}$$

where a_{leaf_o} is the measured a_{leaf} during intense observations (Fig. 2).

In order to reproduce the observed NEE and E values using the SVAT model developed herein, we used the measured temporal variations in $V_{cmax,25}(h_c)$ and LAI with the calibrated k_n ("Control" in Table 2). Control optimized k_n to maximize the sum of the Nash-Sutcliffe efficiency (NSE: Nash and Sutcliffe, 1970) for NEE and E, and was applied separately during the growth period (April–November) and the winter (December–March), as well as for the entire calculation period. Table 1 summarizes the major parameters used for model validation. In addition, three numerical experiments (Cases 1, 2, and 3) were conducted using different inputs for $V_{cmax,25}$ and LAI, as summarized in Table 2. In Cases 1 and 2, the fluxes were calculated using the measured temporal variations in $V_{cmax,25}$ and a constant LAI (annual maximum during the calculation period), and using a constant maximum $V_{cmax,25}$ and the measured variations in LAI, respectively. Case 3 assumed that both $V_{cmax,25}$ and LAI were constant (their annual maximum values). The seasonal variations in the parameters and constants of the annual maximum values are shown in Fig. 1.

Table 2
Description of the SVAT model simulations in which the photosynthetic parameter ($V_{cmax,25}$) and leaf area index (LAI) changed based on measured values.

Cases	$V_{cmax,25}$	LAI
Control	Measured [a]	Measured
Case 1	Measured	MAX [b]
Case 2	MAX	Measured
Case 3	MAX	MAX

[a] "Measured" indicates that the model used the value obtained during the same period as the calculation period.
[b] "MAX" denotes the annual maximum during the calculation period (Fig. 1).

4. Results

4.1. Environmental data and model validation

The daily environmental data for the study period are shown in Fig. 4. As a typical seasonal pattern of P in the snow-free region of Japan, the monthly P amounts were larger during the summer than during the winter, resulting in a substantial seasonal contrast in soil moisture. The maximum T_a reached 35 °C between early August and mid-September 2007 and in July 2008. The minimum T_a was –5 °C in mid-February 2008. T_a and atmospheric vapor pressure deficit (D) exhibited seasonal variations. D and the daily total R_s were low from mid-June to mid-July in 2008, owing to the regular rainy season in Japan.

We compared the measured NEE and E values with the simulated values using the climatic forcing data in Fig. 4 and the measured temporal variations in $V_{cmax,25}$ and LAI (see "Control" in Table 2) (Fig. 5). Assuming that we could only obtain data for ecophysiological traits during the growing season, we also simulated the fluxes using constant $V_{cmax,25}$ and LAI values, which were the average values during the growing season, and the calibrated k_n only during the growing season. Regardless of the assumptions used in the simulation, the SVAT model successfully reproduced canonical forms of both the NEE and E time series throughout the year, thereby highlighting the model's ability to synthesize canopy CO_2 and water vapor transport through stomatal behavior.

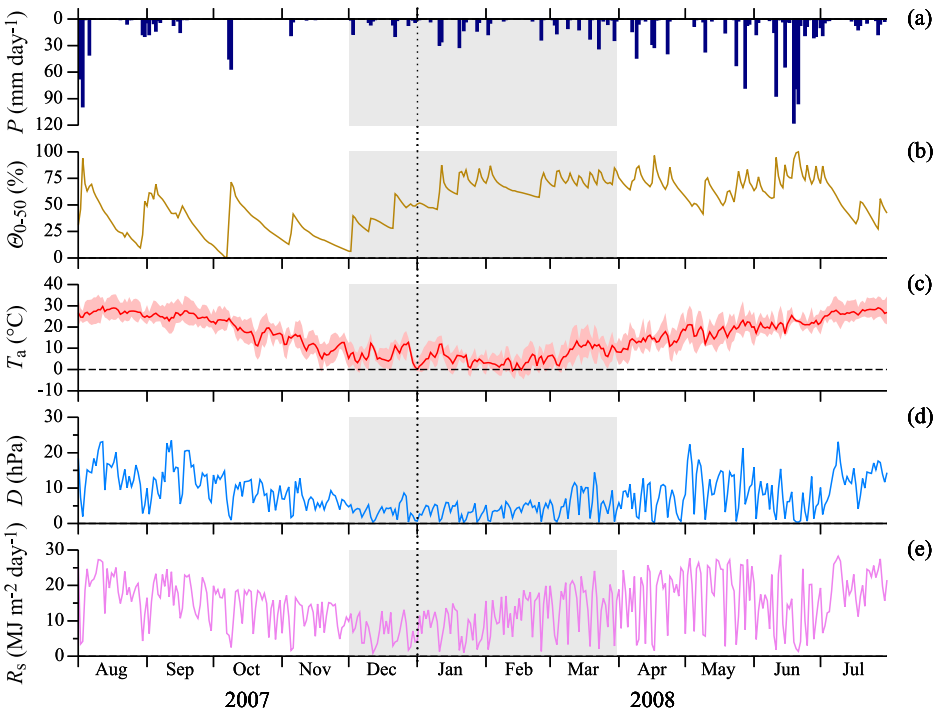

Fig. 4. Annual climate data from August 1, 2007 to July 31, 2008. (a) Daily precipitation (P). (b) Volumetric soil moisture content of the 0–50 cm soil layer, normalized using the difference between the maximum and minimum values during the study period (Θ_{0-50}). (c) Daily mean air temperature (T_a), with the minimum and maximum T_a range for each day. (d) Mean daytime atmospheric humidity deficit (D). (e) Daily total solar radiation (R_s). The shaded zones represent the winter periods.

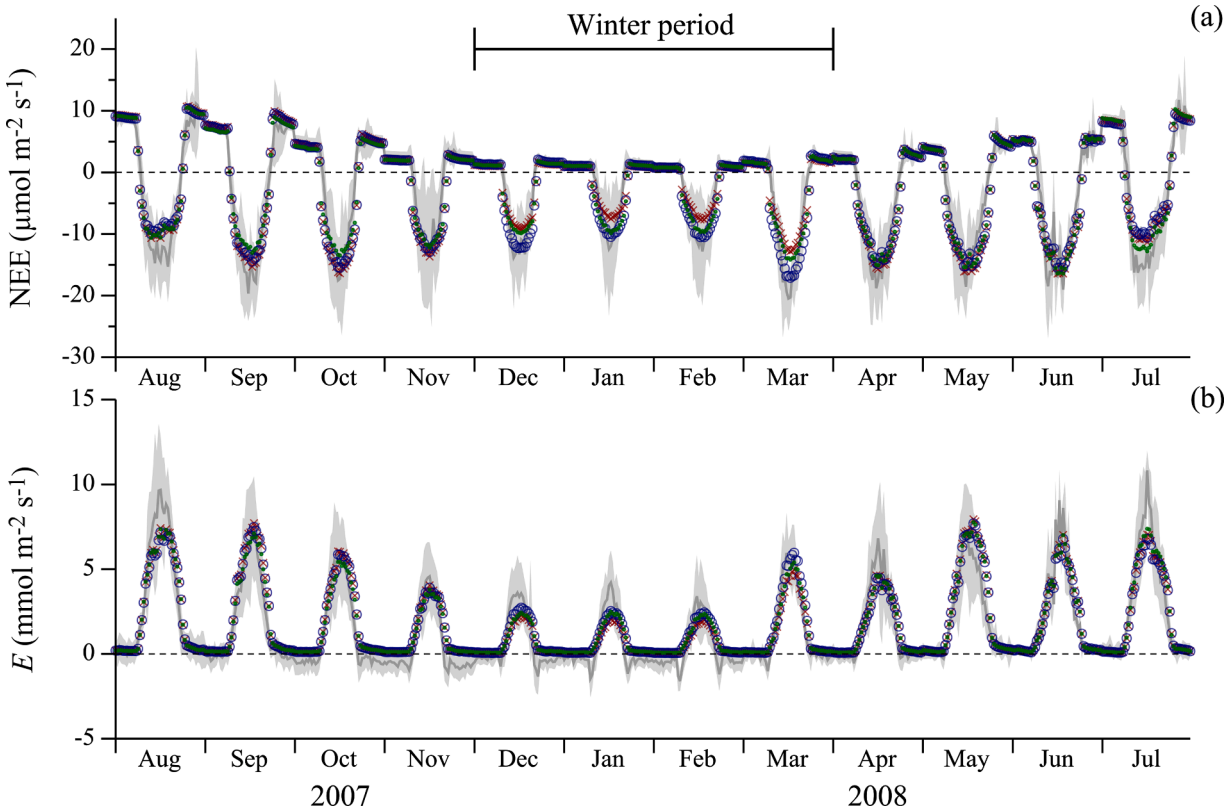

Fig. 5. Monthly mean diurnal cycles of (a) net ecosystem exchange (NEE) and (b) the canopy transpiration rate (E). Solid gray lines with gray zones represent measured mean values with ±1 standard deviation. Simulations were performed using measured temporal variations in $V_{cmax,25}$ and LAI considering seasonal changes in k_n (0.92 for the growth period; 0.47 for the winter) (open circles), maintaining a constant k_n (0.85) (crosses), and using constant $V_{cmax,25}$ (82.1 μmol m^{-2} s^{-1}) and LAI (4.7 m^2 m^{-2}) values with a constant k_n (0.92) throughout the calculation period (closed circles).

Table 3 presents the statistical parameters of the comparisons between the modeled and measured NEE and E values for the three simulation assumptions in the Control. Considering k_n separately for the growing and winter periods improved the reproducibility of the model notably. Simulation using the growing season values of $V_{cmax,25}$, LAI, and k_n had the best reproducibility. It is noteworthy that some partial

Table 3
Regression statistics[a] for comparisons between the measured and modeled net ecosystem CO_2 exchange (NEE) and canopy transpiration rate (E) in the Control.

Period[b]	$V_{cmax,25}$, LAI[c]	k_n[d]	Slope	Intercept	R^2	RMSE	NSE
NEE (μmol m^{-2} s^{-1})							
Growth	Measured	0.92	0.79	–0.62	0.75	4.43	0.74
Growth	Measured	0.85	0.83	–0.71	0.75	4.45	0.74
Growth	Constant	0.92	0.97	0.45	0.76	4.33	0.76
Winter	Measured	0.47	0.74	–1.38	0.72	3.49	0.70
Winter	Measured	0.85	0.54	–0.97	0.71	3.68	0.67
Winter	Constant	0.92	1.11	0.76	0.70	3.56	0.69
E (mmol m^{-2} s^{-1})							
Growth	Measured	0.92	0.78	0.64	0.81	1.26	0.79
Growth	Measured	0.85	0.80	0.64	0.81	1.26	0.79
Growth	Constant	0.92	1.05	–0.40	0.82	1.24	0.80
Winter	Measured	0.47	0.58	0.53	0.69	1.08	0.64
Winter	Measured	0.85	0.47	0.45	0.68	1.13	0.60
Winter	Constant	0.92	1.30	–0.51	0.69	1.10	0.63

[a] The regression model is y = slope x + intercept, where y and x are the measured and modeled fluxes, respectively. The coefficient of determination (R^2), root-mean-squared error (RMSE), and Nash-Sutcliffe efficiency (NSE) are shown in the table.
[b] "Growth" and "Winter" refer to April–November and December–March, respectively (Fig. 1).
[c] "Measured" and "Constant" denote the simulations using the measured temporal variations in the values and using the constants as the mean values during the growth period, respectively (Fig. 1).
[d] See Eq. (19) in the text.

cancellations emerged; higher NEE and E values during the winter with constant higher $V_{cmax,25}$, and LAI values were likely to be reduced due to higher k_n optimized as the growth period value, resulting in an apparently good simulation but with impractical processes. Thus, the simulation with temporal variations in $V_{cmax,25}$, LAI, and k_n determined for the growth period and winter appeared to be more resistant to changes in the simulation scenarios and was adopted as the Control (Table 2).

The Control model estimated annual NEE and E values of 7.516 Mg ha^{-1} of C and 884.2 mm, respectively, which exhibited overestimations of the eddy flux-observed annual NEE and E (i.e., 5.626 Mg ha^{-1} of C and 875.1 mm, respectively). While the simulated fluxes were only obtained from the dry canopy, observed fluxes included those from the wet canopy. Thus, these overestimations occurred because the model tended to overestimate fluxes under rainfall conditions. It should also be noted that there is an intrinsic difficulty in measuring the eddy covariance fluxes under rainfall and those from the wet canopy.

4.2. Numerical experiments

Fig. 6 compares the differences in the monthly and daily mean NEE values between the Control and each Case (Table 2) for the entire canopy, Japanese cedar, and the understory vegetation. Maintenance of the higher Japanese cedar LAI (Case 1) slightly enhanced the productivity of the Japanese cedar, but reduced that of the understory vegetation by increasing shade produced by the upper canopy. This resulted in a small reduction in total ecosystem productivity. Only an increase in the Japanese cedar $V_{cmax,25}$ (Case 2) increased the productivity of the Japanese cedar, particularly from the winter to early summer. We found that the experiment with mixed effects of Cases 1 and 2 (i.e., Case 3) yielded almost the same results as Case 2, suggesting that seasonal variations in $V_{cmax,25}$ are a determining factor for the productivity of Japanese cedar and the entire canopy.

Throughfall and stemflow observations at the study site allowed us to estimate canopy interception (I_c) related to concurrent precipitation (Kumagai et al., 2014; Shimizu et al., 2015). Following this, we examined how ecosystem water resources, including soil moisture and effective precipitation (i.e., $P - I_c$), sustain forest water use, E, for each Case (Fig. 7). The smallest differences were observed for E between Cases, including the Control. In September, November, and July, the

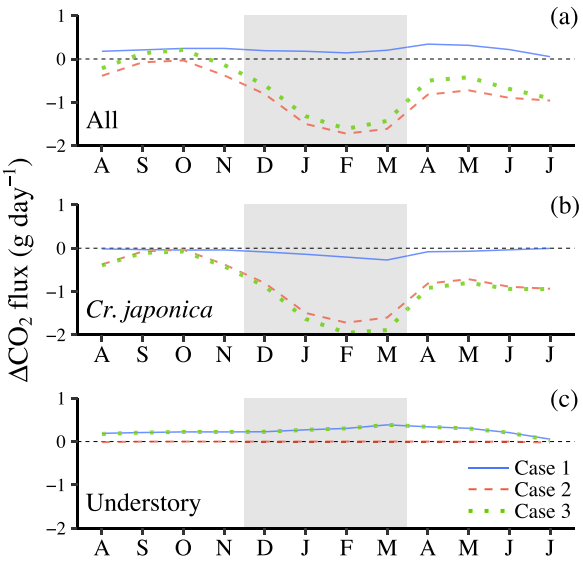

Fig. 6. Monthly mean differences in daily net ecosystem exchange (ΔCO_2 flux) between the Control and each Case (Table 2) for (a) the entire canopy, (b) Japanese cedar, and (c) the understory vegetation. The shaded zones represent the winter periods.

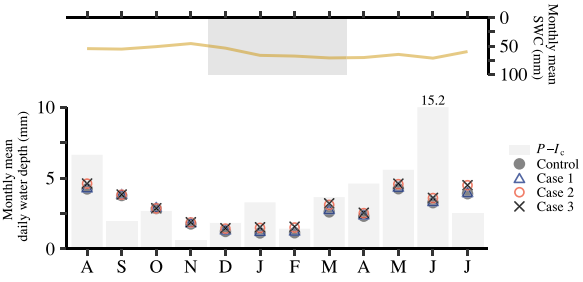

Fig. 7. Upper panel: monthly mean soil water content (SWC). The shaded zone represents the winter period. The lower panel shows monthly mean daily water depths of effective precipitation (precipitation minus intercepted rainwater: $P - I_c$) and transpiration rates for each Case (Table 2). The number at the top of the bar denotes the value of $P - I_c$ for a particular month.

water supply to the soil ($P - I_c$) was unable to satisfy the water demands of E; however, soil moisture was stable and ample throughout the year because the ecosystem's water resources during those months could be retained from previous months. This indicates that the ecosystem's water resources cannot be a limiting factor for fluxes at this study site, despite slight increases in E in Cases 2 and 3.

It is worth investigating why the highest $V_{cmax,25}$ during the growth period was not maintained from winter to early summer when higher productivity occurred, even during the winter Fig. 6b). It is logical to assume that leaf nitrogen dynamics could be key for answering this question, as $V_{cmax,25}$ can be related to the nitrogen content per leaf area (N_{leaf}) (Niinements and Tenhunen, 1997). In this study, we estimated the ground area-based leaf nitrogen usage, $\int_0^{h_c} N_{leaf}(z)a_{leaf}(z)dz$ by using the linear relationship between $V_{cmax,25}$ and N_{leaf} reported by Tobita et al. (2015) and Eqs. (19) and ((20) (Fig. 8a). We found that maintaining the highest $V_{cmax,25}$ during the winter led to an overuse of leaf nitrogen. In addition, we estimated the nitrogen use efficiency (NUE) and water use efficiency (WUE), demonstrating that a constant high $V_{cmax,25}$ value substantially exacerbated NUE, but slightly improved WUE (Fig. 8b, c).

5. Discussion

LAI and $V_{cmax,25}$ are crucial biotic parameters used to simulate

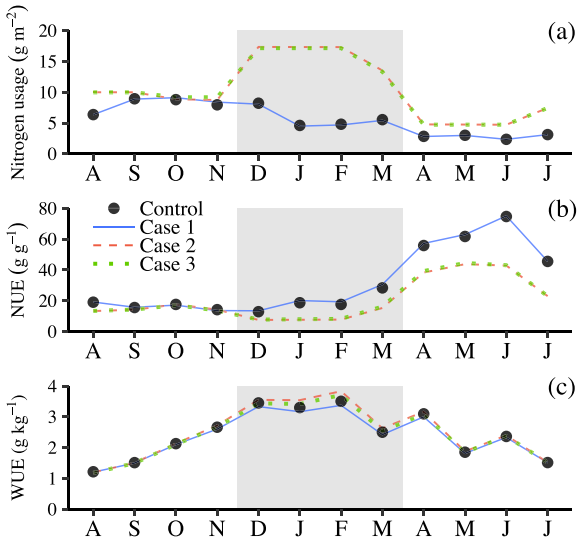

Fig. 8. Monthly values of ground area-based (a) leaf nitrogen usage, (b) nitrogen use efficiency (NUE), and (c) water use efficiency (WUE) for Japanese cedar in each Case (Table 2). The shaded zones represent the winter periods.

canopy-level CO_2 and H_2O exchanges in land surface models and must be determined prior to simulation. Nevertheless, very few direct observations of LAI and $V_{cmax,25}$ time series are available for evergreen conifer trees, since their evergreen nature allows us to intuitively assume that the seasonal variations in LAI and $V_{cmax,25}$ are small (Wang et al., 2019). Luo et al. (2019) found that simulated GPP results for evergreen conifer forests were worse when considering the seasonality of LAI and $V_{cmax,25}$; however, we inferred that this might be due to underestimation of the satellite-derived LAI. Wang et al. (2019) demonstrated that considering seasonality was important for LAI, the corrected satellite-derived LAI value, and $V_{cmax,25}$, which improved the simulated GPP of evergreen conifer forests. To the best of our knowledge, direct observations of seasonal LAI and $V_{cmax,25}$ trajectories for Japanese cedar forests have not been performed (cf. Miyazawa et al., 2017).

We obtained minor seasonal variations in LAI (i.e., a higher LAI during the growth period than in winter) with a somewhat constant LAI (Fig. 1a). This might be explained by the small leaf turnover rate estimated from the long leaf lifespan of the Japanese cedar (~5 years) and the timing of shoot generation during the early growth period (according to personal observations). In general, satellite-derived LAI data used to drive land surface models for evergreen conifer forests, such as the Copernicus Global Land Service GEOV1 LAI product (Baret et al., 2013) and the University of Toronto's LAI product Version 2 (Gonsamo and Chen, 2014) tend to underestimate LAI appreciably during the winter (~0). Wang et al. (2019) successfully corrected satellite-derived evergreen conifer forest LAI values using leaf lifespan information. The LAI observation results obtained herein were consistent with these corrections. In the studied Japanese cedar forest ecosystem, even small seasonal variations in LAI (Fig. 1a) had ecological implications. Maintaining a higher LAI throughout the year has small advantages for Japanese cedar trees and large disadvantages for the understory vegetation (Fig. 6).

Note that not much data is available regarding directly observed evergreen conifer $V_{cmax,25}$ values (cf. Walker et al., 2014). In particular, yearlong $V_{cmax,25}$ data were found only in Han et al. (2008) and Miyazawa et al. (2017). We estimated the global trends of evergreen conifer shoot-projected area-based $V_{cmax,25}$ from the global leaf ecophysiology dataset (Walker et al., 2014) using previous studies (e.g., Bauer et al., 2001; Bown et al., 2007; Carswell et al., 2005; Han et al., 2008; Manter et al., 2005; Merilo et al., 2006; Porté and Loustau, 1998; Tissue et al., 2005). This estimate resulted in a value of 88.6 ± 57.6 (mean ± standard deviation) μmol m^{-2} s^{-1}. The $V_{cmax,25}$ values observed in this study (Table 1; 50.8–98.4 μmol m^{-2} s^{-1}) were comparable to this global estimate.

Han et al. (2008) demonstrated evident seasonal variations in $V_{cmax,25}$ for *Pinus densiflora* Sieb. et Zucc., ranging from ~60 μmol m^{-2} s^{-1} (growing period) to ~20 μmol m^{-2} s^{-1} (winter). In addition, Han et al. (2003) observed a seasonal trend in $V_{cmax,25}$ for Japanese cedar trees of 63.3 (August) and 34.4 μmol m^{-2} s^{-1} (February). In contrast, Miyazawa et al. (2017) observed little seasonality in $V_{cmax,25}$ (~50–60 μmol m^{-2} s^{-1}) throughout the year in another Japanese cedar plantation. Indices for the photosynthetic traits of evergreen conifer forests have been documented using satellite (e.g., Luo et al., 2019; Wang et al., 2019) or near-surface (e.g., Bowling et al., 2018; Seyednasrollah et al., 2021) remote sensing data. These studies successfully inferred seasonal changes in leaf chlorophyll content and $V_{cmax,25}$. Thus, the apparent seasonal variations in $V_{cmax,25}$ observed in this study (Fig. 1b; Table 1) are consistent with the general findings regarding seasonal variations in $V_{cmax,25}$ for evergreen conifers.

To reproduce the observed seasonal variations in NEE and *E*, k_n was calibrated to be 0.92 and 0.47 in the growth and winter periods, respectively (Table 1). Since we assumed a linear relationship between $V_{cmax,25}$ and N_{leaf}, the photosynthetic nitrogen distribution attenuation coefficient (K_b) in the global meta-analysis of Hikosaka et al. (2016) could be equivalent to k_n. Hikosaka et al. (2016) suggested that GPP simulated with a terrestrial carbon flux model is sensitive to K_b, which ranged from 0.15 to 0.40 for woody species in their meta-analysis. The k_n values estimated in this study were within the range of reported values for crop species (i.e., 0.1–1.2), rather than those of tree species (Hikosaka et al., 2016). Farquhar (1989) demonstrated that the maximum photosynthesis rate is proportional to the relative light intensity along the canopy depth to maximize canopy photosynthesis. Therefore, because leaf area density is concentrated in the upper crown of the trees (Fig. 2), the k_n values estimated in this study might be higher than the expected values.

From the quantitative experiments conducted in this study, we found that maintaining a high $V_{cmax,25}$ throughout the year, even during the winter, led to higher productivity (Fig. 6); however, $V_{cmax,25}$ decreased in the winter (Fig. 1b). It was evident that the ecosystem's water resources could not be a limiting factor for vegetation activities at this study site (Fig. 7). Then we considered nitrogen availability, which often controls net primary productivity (e.g., Goll et al., 2012). In order to maintain high $V_{cmax,25}$ values during the winter, Japanese cedar apparently overused the nitrogen resources and exacerbated the NUE with an almost unchanged WUE (Fig. 8). It would be more difficult to cover overused nitrogen during the winter, as the mineral nitrogen supply from soil organic matter decomposition is insufficient under low-temperature conditions (e.g., Wieder et al., 2013). Hence, a decrease in $V_{cmax,25}$ during the winter appears to be necessary for sustaining the forest ecosystem.

Another possibility is that long-term acclimation to low temperatures might cause the $V_{cmax,25}$ values to be lower during the winter. Han et al. (2003) found that xanthophyll rhodoxanthin, which plays a photoprotective role during cold acclimation, accumulated in cedar needle leaves during the winter, inducing reddish-brown leaves with reduced $V_{cmax,25}$ values. A reddish-brown upper canopy was observed at the study site (Kumagai et al., 2008), from which we inferred that cold acclimation was a major reason for the decreases in $V_{cmax,25}$ and NEE during the winter. Furthermore, Han et al. (2004) suggested that Japanese cedar trees accumulate rhodoxanthin and have decreased electron transport rates and photochemical quenching in sun-exposed leaves during the winter, but do not accumulate rhodoxanthin or consistent photosynthetic activity in the shaded leaves. This also implies that the lower k_n during the winter could be due to reduced and maintained photosynthetic activity in the upper and lower shaded parts of the canopy, respectively.

6. Conclusions

Using a combination of annual eddy covariance fluxes and leaf ecophysiology observations and the multi-layer SVAT model, we examined how seasonal variations in $V_{cmax,25}$ affected canopy CO_2 and H_2O fluxes and ecosystem productivity in a Japanese cedar plantation. We arrived at conclusions regarding the ecological meaning of the aforementioned seasonal variations in $V_{cmax,25}$ and its relationship with the reddish-brown canopy color. Canopy color information provides a useful metric for monitoring and modeling photosynthetic activity in global evergreen forests (e.g., Bowling et al., 2018; Seyednasrollah et al., 2021). The SVAT model can consider the effect of the canopy structure and detailed leaf-level physiology (including vertical profiles within the canopy) on the computed outputs. Hence, numerical experiments using the SVAT model and a simple method to predict $V_{cmax,25}$ (such as canopy color information) would allow us to investigate the impacts of forest management on carbon and water cycling (e.g., determining best practices for balancing forest production and environmental conservation).

Declaration of Competing Interest

The authors declare that they have no known competing financial interests or personal relationships that could have appeared to influence the work reported in this paper.

Data Availability

Data will be made available on request.

Acknowledgments

The maintenance of the KHEW is supported by the Kyushu Research Center of the Forestry and Forest Products Research Institute (FFPRI) and the National Forests in the Kyushu Office. This work was supported by Grants-in-Aid for Scientific Research (Nos. 21H05316 and 17H01477) from the Ministry of Education, Culture, Sports, Science and Technology, Japan. This study was part of "The Long-Term CO_2 Flux Observation Project (#200303)" supported by the FFPRI. We are grateful to Kyoichi Otsuki, Sayaka Aoki, and Natsuko Yoshifuji for logistical support and help with fieldwork.

Supplementary materials

Supplementary material associated with this article can be found, in the online version, at doi:10.1016/j.ecolmodel.2022.110271.

References

Badger, M.R., Collatz, G.J., 1977. Studies on the Kinetic Mechanism of Ribulose-1,5-Bisphosphate Carboxylase and Oxygenase Reactions, with Particular Reference to the Effect of Temperature on Kinetic Parameters, 76. Carnegie Institute of Washington Yearbook, pp. 355–361.

Baldocchi, D., Meyers, T., 1998. On using eco-physiological, micrometeorological and biogeochemical theory to evaluate carbon dioxide, water vapor and trace gas fluxes over vegetation: a perspective. Agric. For. Meteorol. 90, 1–25, 10/c2rxpn.

Baret, F., Weiss, M., Lacaze, R., Camacho, F., Makhmara, H., Pacholcyzk, P., Smets, B., 2013. GEOV1: *LAI* and *FAPAR* essential climate variables and *FCOVER* global time series capitalizing over existing products. Part1: principles of development and production. Remote Sens. Environ. 137, 299–309. https://doi.org/10.1016/j.rse.2012.12.027.

Bauer, G.A., Berntson, G.M., Bazzaz, F.A., 2001. Regenerating temperate forests under elevated CO_2 and nitrogen deposition: comparing biochemical and stomatal limitation of photosynthesis. New Phytol. 152, 249–266. https://doi.org/10.1046/j.0028-646X.2001.00255.x.

Bernacchi, C.J., Pimentel, C., Long, S.P., 2003. *In vivo* temperature response functions of parameters required to model RuBP-limited photosynthesis. Plant Cell Environ. 26, 1419–1430. https://doi.org/10.1046/j.0016-8025.2003.01050.x.

Bernacchi, C.J., Singsaas, E.L., Pimentel, C., Jr, A.R.P., Long, S.P., 2001. Improved temperature response functions for models of Rubisco-limited photosynthesis. Plant Cell Environ. 24, 253–259. https://doi.org/10.1111/j.1365-3040.2001.00668.x.

Bonan, G.B., Patton, E.G., Finnigan, J.J., Baldocchi, D.D., Harman, I.N., 2021. Moving beyond the incorrect but useful paradigm: reevaluating big-leaf and multi-layer plant canopies to model biosphere-atmosphere fluxes – a review. Agric. For. Meteorol. 306, 108435 https://doi.org/10.1016/j.agrformet.2021.108435.

Bourdeau, P.F., 1959. Seasonal variations of the photosynthetic efficiency of evergreen conifers. Ecology 40, 63–67. https://doi.org/10.2307/1929923.

Bowling, D.R., Logan, B.A., Hufkens, K., Aubrecht, D.M., Richardson, A.D., Burns, S.P., Anderegg, W.R.L., Blanken, P.D., Eiriksson, D.P., 2018. Limitations to winter and spring photosynthesis of a Rocky Mountain subalpine forest. Agric. For. Meteorol. 252, 241–255. https://doi.org/10.1016/j.agrformet.2018.01.025.

Bown, H.E., Watt, M.S., Clinton, P.W., Mason, E.G., Richardson, B., 2007. Partititioning concurrent influences of nitrogen and phosphorus supply on photosynthetic model parameters of *Pinus radiata*. Tree Physiol. 27, 335–344. https://doi.org/10.1093/treephys/27.3.335.

Campbell, G.S., Norman, J., 1998. An Introduction to Environmental Biophysics, 2nd ed. Springer-Verlag, New York. https://doi.org/10.1007/978-1-4612-1626-1.

Carswell, F.E., Whitehead, D., Rogers, G.N.D., Mcseveny, T.M., 2005. Plasticity in photosynthetic response to nutrient supply of seedlings from a mixed conifer-angiosperm forest. Austral. Ecol. 30, 426–434. https://doi.org/10.1111/j.1442-9993.2005.01486.x.

Collatz, G.J., Ball, J.T., Grivet, C., Berry, J.A., 1991. Physiological and environmental regulation of stomatal conductance, photosynthesis and transpiration: a model that includes a laminar boundary layer. Agric. For. Meteorol. 54, 107–136. https://doi.org/10.1016/0168-1923(91)90002-8.

de Pury, D.G.G., Farquhar, G.D., 1997. Simple scaling of photosynthesis from leaves to canopies without the errors of big-leaf models. Plant Cell Environ. 20, 537–557, 10/fr9jhj.

Egusa, T., Kumagai, T., Shiraishi, N., 2020. Carbon stock in Japanese forests has been greatly underestimated. Sci. Rep. 10, 7895. https://doi.org/10.1038/s41598-020-64851-2.

Escudero, A., Mediavilla, S., 2003. Decline in photosynthetic nitrogen use efficiency with leaf age and nitrogen resorption as determinants of leaf life span. J. Ecol. 91, 880–889. https://doi.org/10.1046/j.1365-2745.2003.00818.x.

Farquhar, G., Wong, S., 1984. An empirical model of stomatal conductance. Aust. J. Plant Physiol. 11, 191–210. https://doi.org/10.1071/PP9840191.

Farquhar, G.D., 1989. Models of Integrated Photosynthesis of Cells and Leaves. Philos. Trans. R. Soc. Lond. B. Biol. Sci. 323, 357–367. https://doi.org/10.1098/rstb.1989.0016.

Farquhar, G.D., von Caemmerer, S., Berry, J.A., 1980. A biochemical model of photosynthetic CO_2 assimilation in leaves of C_3 species. Planta 149, 78–90, 10/fs9dpz.

Goll, D.S., Brovkin, V., Parida, B.R., Reick, C.H., Kattge, J., Reich, P.B., van Bodegom, P. M., Niinemets, Ü., 2012. Nutrient limitation reduces land carbon uptake in simulations with a model of combined carbon, nitrogen and phosphorus cycling. Biogeosciences 9, 3547–3569. https://doi.org/10.5194/bg-9-3547-2012.

Gonsamo, A., Chen, J.M., 2014. Improved LAI algorithm implementation to MODIS data by incorporating background, topography, and foliage clumping information. IEEE Trans. Geosci. Remote Sens. 52, 1076–1088. https://doi.org/10.1109/TGRS.2013.2247405.

Goudriaan, J., 1977. Crop Micrometeorology: A Simulation Study. Cent. for Agric. Publ. and Doc., Wageningen.

Han, Q., Katahata, S., Kakubari, Y., Mukai, Y., 2004. Seasonal changes in the xanthophyll cycle and antioxidants in sun-exposed and shaded parts of the crown of *Cryptomeria japonica* in relation to rhodoxanthin accumulation during cold acclimation. Tree Physiol. 24, 609–616, 10/fxkzhd.

Han, Q., Kawasaki, T., Nakano, T., Chiba, Y., 2008. Leaf-age effects on seasonal variability in photosynthetic parameters and its relationships with leaf mass per area and leaf nitrogen concentration within a *Pinus densiflora* crown. Tree Physiol. 28, 551–558. https://doi.org/10.1093/treephys/28.4.551.

Han, Q., Mukai, Y., 1999. Cold acclimation and photoinhibition of photosynthesis accompanied by needle color changes in *Cryptomeria japonica* during the winter. J. For. Res. 4, 229–234, 10/db9b53.

Han, Q., Shinohara, K., Kakubari, Y., Mukai, Y., 2003. Photoprotective role of rhodoxanthin during cold acclimation in *Cryptomeria japonica*. Plant Cell Environ. 26, 715–723, 10/bts364.

Heskel, M.A., Atkin, O.K., Turnbull, M.H., Griffin, K.L., 2013. Bringing the Kok effect to light: a review on the integration of daytime respiration and net ecosystem exchange. Ecosphere 4 art9810/ggfktj.

Hikosaka, K., Anten, N.P.R., Borjigidai, A., Kamiyama, C., Sakai, H., Hasegawa, T., Oikawa, S., Iio, A., Watanabe, M., Koike, T., Nishina, K., Ito, A., 2016. A meta-analysis of leaf nitrogen distribution within plant canopies. Ann. Bot. 118, 239–247. https://doi.org/10.1093/aob/mcw099.

Ishizuka, S., Sakata, T., Sawata, S., Ikeda, S., Takenaka, C., Tamai, N., Sakai, H., Shimizu, T., Kan-Na, K., Onodera, S., Tanaka, N., Takahashi, M., 2006. High potential for increase in CO_2 flux from forest soil surface due to global warming in cooler areas of Japan. Ann. For. Sci. 63, 537–546, 10/bxxpcb.

Japan Forestry Agency, 2021. Annual Report on Forest and Forestry in Japan: Fiscal Year 2020. The ministry of agriculture. For. Fish. Jpn. Tokyo (in Japanese).

Katul, G.G., Albertson, J.D., 1999. Modeling CO_2 sources, sinks, and fluxes within a forest canopy. J. Geophys. Res. Atmosph. 104, 6081–6091. https://doi.org/10.1029/1998JD200114.

Kondo, J., Watanabe, T., 1992. Studies on the bulk transfer coefficients over a vegetated surface with a multi-layer energy budget model. J. Atmosph. Sci. 49, 2183–2199. https://doi.org/10.1175/1520-0469(1992)049<2183:SOTBTC>2.0.CO;2.

Kumagai, T., Ichie, T., Yoshimura, M., Yamashita, M., Kenzo, T., Saitoh, T.M., Ohashi, M., Suzuki, M., Koike, T., Komatsu, H., 2006. Modeling CO_2 exchange over a

Bornean tropical rain forest using measured vertical and horizontal variations in leaf-level physiological parameters and leaf area densities. J. Geophys. Res. Atmosph. 111 https://doi.org/10.1029/2005JD006676 n/a-n/a.
Kumagai, T., Kume, T., 2012. Influences of diurnal rainfall cycle on CO_2 exchange over Bornean tropical rainforests. Ecol. Model. 246, 91–98. https://doi.org/10.1016/j.ecolmodel.2012.07.014.
Kumagai, T., Mudd, R.G., Miyazawa, Y., Liu, W., Giambelluca, T.W., Kobayashi, N., Lim, T.K., Jomura, M., Matsumoto, K., Huang, M., Chen, Q., Ziegler, A., Yin, S., 2013. Simulation of canopy CO_2/H_2O fluxes for a rubber (*Hevea brasiliensis*) plantation in central Cambodia: The effect of the regular spacing of planted trees. Ecol. Model. 265, 124–135. https://doi.org/10.1016/j.ecolmodel.2013.06.016.
Kumagai, T., Tateishi, M., Miyazawa, Y., Kobayashi, M., Yoshifuji, N., Komatsu, H., Shimizu, T., 2014. Estimation of annual forest evapotranspiration from a coniferous plantation watershed in Japan (1): Water use components in Japanese cedar stands. J. Hydrol. 508, 66–76. https://doi.org/10.1016/j.jhydrol.2013.10.047.
Kumagai, T., Tateishi, M., Shimizu, T., Otsuki, K., 2008. Transpiration and canopy conductance at two slope positions in a Japanese cedar forest watershed. Agric. For. Meteorol. 148, 1444–1455. https://doi.org/10.1016/j.agrformet.2008.04.010.
Kumarathunge, D.P., Medlyn, B.E., Drake, J.E., Rogers, A., Tjoelker, M.G., 2019. No evidence for triose phosphate limitation of light-saturated leaf photosynthesis under current atmospheric CO_2 concentration. Plant Cell Environ. 42, 3241–3252. https://doi.org/10.1111/pce.13639.
Lai, C.-T., Katul, G., Ellsworth, D., Oren, R., 2000. Modelling vegetation-atmosphere CO_2 exchange by a coupled Eulerian-Langrangian approach. Bound.-Layer Meteorol 95, 91–122. https://doi.org/10.1023/A:1002473906184.
Lawrence, D.M., Fisher, R.A., Koven, C.D., Oleson, K.W., Swenson, S.C., Bonan, G., Collier, N., Ghimire, B., Kampenhout, L.van, Kennedy, D., Kluzek, E., Lawrence, P.J., Li, F., Li, H., Lombardozzi, D., Riley, W.J., Sacks, W.J., Shi, M., Vertenstein, M., Wieder, W.R., Xu, C., Ali, A.A., Badger, A.M., Bisht, G., Broeke, M.van den, Brunke, M.A., Burns, S.P., Buzan, J., Clark, M., Craig, A., Dahlin, K., Drewniak, B., Fisher, J.B., Flanner, M., Fox, A.M., Gentine, P., Hoffman, F., Keppel-Aleks, G., Knox, R., Kumar, S., Lenaerts, J., Leung, L.R., Lipscomb, W.H., Lu, Y., Pandey, A., Pelletier, J.D., Perket, J., Randerson, J.T., Ricciuto, D.M., Sanderson, B.M., Slater, A., Subin, Z.M., Tang, J., Thomas, R.Q., Martin, M.V., Zeng, X., 2019. The community land model version 5: description of new features, benchmarking, and impact of forcing uncertainty. J. Adv. Model. Earth Syst. https://doi.org/10.1029/2018MS001583 n/a.
Leuning, R., Kelliher, F.M., Pury, D.G.G., Schulze, E.-D., 1995. Leaf nitrogen, photosynthesis, conductance and transpiration: scaling from leaves to canopies. Plant Cell Environ. 18, 1183–1200. https://doi.org/10.1111/j.1365-3040.1995.tb00628.x.
Lin, Y.-S., Medlyn, B.E., Duursma, R.A., Prentice, I.C., Wang, H., Baig, S., Eamus, D., de Dios, V.R., Mitchell, P., Ellsworth, D.S., de Beeck, M.O., Wallin, G., Uddling, J., Tarvainen, L., Linderson, M.-L., Cernusak, L.A., Nippert, J.B., Ocheltree, T.W., Tissue, D.T., Martin-StPaul, N.K., Rogers, A., Warren, J.M., De Angelis, P., Hikosaka, K., Han, Q., Onoda, Y., Gimeno, T.E., Barton, C.V.M., Bennie, J., Bonal, D., Bosc, A., Löw, M., Macinins-Ng, C., Rey, A., Rowland, L., Setterfield, S.A., Tausz-Posch, S., Zaragoza-Castells, J., Broadmeadow, M.S.J., Drake, J.E., Freeman, M., Ghannoum, O., Hutley, L.B., Kelly, J.W., Kikuzawa, K., Kolari, P., Koyama, K., Limousin, J.-M., Meir, P., Lola da Costa, A.C., Mikkelsen, T.N., Salinas, N., Sun, W., Wingate, L., 2015. Optimal stomatal behaviour around the world. Nat. Clim. Change 5, 459–464. https://doi.org/10.1038/nclimate2550.
Luo, X., Croft, H., Chen, J.M., He, L., Keenan, T.F., 2019. Improved estimates of global terrestrial photosynthesis using information on leaf chlorophyll content. Glob. Change Biol. 25, 2499–2514. https://doi.org/10.1111/gcb.14624.
Manter, D.K., Kavanagh, K.L., Rose, C.L., 2005. Growth response of Douglas-fir seedlings to nitrogen fertilization: importance of Rubisco activation state and respiration rates. Tree Physiol. 25, 1015–1021. https://doi.org/10.1093/treephys/25.8.1015.
Manzoni, S., Katul, G., Fay, P.A., Polley, H.W., Porporato, A., 2011. Modeling the vegetation–atmosphere carbon dioxide and water vapor interactions along a controlled CO_2 gradient. Ecol. Model. 222, 653–665. https://doi.org/10.1016/j.ecolmodel.2010.10.016.
Medlyn, B.E., Duursma, R.A., Eamus, D., Ellsworth, D.S., Prentice, I.C., Barton, C.V.M., Crous, K.Y., De Angelis, P., Freeman, M., Wingate, L., 2011. Reconciling the optimal and empirical approaches to modelling stomatal conductance. Glob. Change Biol. 17, 2134–2144. https://doi.org/10.1111/j.1365-2486.2010.02375.x.
Merilo, E., Heinsoo, K., Kull, O., Söderbergh, I., Lundmark, T., Koppel, A., 2006. Leaf photosynthetic properties in a willow (*Salix viminalis* and *Salix dasyclados*) plantation in response to fertilization. Eur. J. For. Res. 125, 93–100. https://doi.org/10.1007/s10342-005-0073-7.
Miner, G.L., Bauerle, W.L., Baldocchi, D.D., 2017. Estimating the sensitivity of stomatal conductance to photosynthesis: a review. Plant Cell Environ. 40, 1214–1238. https://doi.org/10.1111/pce.12871.
Miyazawa, Y., Inoue, A., Maruyama, A., Otsuki, K., Giambelluca, T.W., 2017. Transpiration of trees in a cool temperate forest on Mt. Aso, Japan: comparison of model simulation and measurements. Ecol. Res. 32, 547–557. https://doi.org/10.1007/s11284-017-1471-2.
Miyazawa, Y., Tateishi, M., Komatsu, H., Kumagai, T., Otsuki, K., 2011. Are measurements from excised leaves suitable for modeling diurnal patterns of gas exchange of intact leaves? Hydrol. Process. 25, 2924–2930. https://doi.org/10.1002/hyp.8107.
Momiyama, H., Kumagai, T., Egusa, T., 2021. Model analysis of forest thinning impacts on the water resources during hydrological drought periods. For. Ecol. Manag. 499, 119593 https://doi.org/10.1016/j.foreco.2021.119593.
Nash, J.E., Sutcliffe, J.V., 1970. River flow forecasting through conceptual models part I — A discussion of principles. J. Hydrol. 10, 282–290. https://doi.org/10.1016/0022-1694(70)90255-6.
Niinemets, Ü., Tenhunen, J.D., 1997. A model separating leaf structural and physiological effects on carbon gain along light gradients for the shade-tolerant species *Acer saccharum*. Plant Cell Environ. 20, 845–866. https://doi.org/10.1046/j.1365-3040.1997.d01-133.x.
Ohsumi, K., 2018. Historical changes of forests in Japan. In: Nakashizuka, T., Kikuzawa, K. (Eds.), Series of Forest Science 1: Changes in Forests in Relation to Human. Kyoritsu Shuppan Co., Ltd., Japan, pp. 68–123 (in Japanese).
Porté, A., Loustau, D., 1998. Variability of the photosynthetic characteristics of mature needles within the crown of a 25-year-old *Pinus pinaster*. Tree Physiol. 18, 223–232. https://doi.org/10.1093/treephys/18.4.223.
Saitoh, T.M., Tamagawa, I., Muraoka, H., Lee, N.-Y.M., Yashiro, Y., Koizumi, H., 2010. Carbon dioxide exchange in a cool-temperate evergreen coniferous forest over complex topography in Japan during two years with contrasting climates. J. Plant Res. 123, 473–483. https://doi.org/10.1007/s10265-009-0308-7.
Sellers, P.J., Randall, D.A., Collatz, G.J., Berry, J.A., Field, C.B., Dazlish, D.A., Zhang, C., Collelo, G.D., Bounoua, L., 1996. A revised land surface parameterization (SiB2) for atmospheric GCMs. Part I: model formulation. J. Clim. 9, 676–705. https://doi.org/10.1175/1520-0442(1996)009%3C0676:ARLSPF%3E2.0.CO;2.
Seyednasrollah, B., Bowling, D.R., Cheng, R., Logan, B.A., Magney, T.S., Frankenberg, C., Yang, J.C., Young, A.M., Hufkens, K., Arain, M.A., Black, T.A., Blanken, P.D., Bracho, R., Jassal, R., Hollinger, D.Y., Law, B.E., Nesic, Z., Richardson, A.D., 2021. Seasonal variation in the canopy color of temperate evergreen conifer forests. New Phytol. 229, 2586–2600. https://doi.org/10.1111/nph.17046.
Shimizu, T., Kumagai, T., Kobayashi, M., Tamai, K., Iida, S., Kabeya, N., Ikawa, R., Tateishi, M., Miyazawa, Y., Shimizu, A., 2015. Estimation of annual forest evapotranspiration from a coniferous plantation watershed in Japan (2): Comparison of eddy covariance, water budget and sap-flow plus interception loss. J. Hydrol. 522, 250–264. https://doi.org/10.1016/j.jhydrol.2014.12.021.
Tamai, K., 2010. Effects of environmental factors and soil properties on topographic variations of soil respiration. Biogeosciences 7, 1133–1142. https://doi.org/10.5194/bgd-6-10935-2009.
Tissue, D.T., Griffin, K.L., Turnbull, M.H., Whitehead, D., 2005. Stomatal and non-stomatal limitations to photosynthesis in four tree species in a temperate rainforest dominated by *Dacrydium cupressinum* in New Zealand. Tree Physiol. 25, 447–456. https://doi.org/10.1093/treephys/25.4.447.
Tobita, H., Kitao, M., Saito, S., Kabeya, D., Kawasaki, T., Yazaki, K., Komatsu, M., Kajimoto, T., 2015. The relationships between nitrogen content in needles and photosynthetic parameter within crown of *Cryptomeria japonica*. Kanto J. For. Res. 66, 13–16 (in Japanese with English abstract).
von Caemmerer, S., Evans, J.R., Hudson, G.S., Andrews, T.J., 1994. The kinetics of ribulose-1,5-bisphosphate carboxylase/oxygenase *in vivo* inferred from measurements of photosynthesis in leaves of transgenic tobacco. Planta 195, 88–97. https://doi.org/10.1007/BF00206296.
von Caemmerer, S., Farquhar, G.D., 1981. Some relationships between the biochemistry of photosynthesis and the gas exchange of leaves. Planta 153, 376–387. https://doi.org/10.1007/BF00384257.
Walker, A.P., Beckerman, A.P., Gu, L., Kattge, J., Cernusak, L.A., Domingues, T.F., Scales, J.C., Wohlfahrt, G., Wullschleger, S.D., Woodward, F.I., 2014. The relationship of leaf photosynthetic traits – V_{cmax} and J_{max} – to leaf nitrogen, leaf phosphorus, and specific leaf area: a meta-analysis and modeling study. Ecol. Evol. 4, 3218–3235. https://doi.org/10.1002/ece3.1173.
Wang, R., Chen, J.M., Luo, X., Black, A., Arain, A., 2019. Seasonality of leaf area index and photosynthetic capacity for better estimation of carbon and water fluxes in evergreen conifer forests. Agric. For. Meteorol. 279, 107708 https://doi.org/10.1016/j.agrformet.2019.107708.
Wieder, W.R., Bonan, G.B., Allison, S.D., 2013. Global soil carbon projections are improved by modelling microbial processes. Nat. Clim. Change 3, 909–912. https://doi.org/10.1038/nclimate1951.
Wilson, K.B., Baldocchi, D.D., Hanson, P.J., 2001. Leaf age affects the seasonal pattern of photosynthetic capacity and net ecosystem exchange of carbon in a deciduous forest. Plant Cell Environ. 24, 571–583. https://doi.org/10.1046/j.0016-8025.2001.00706.x.
Wohlfahrt, G., Bahn, M., Haslwanter, A., Newesely, C., Cernusca, A., 2005. Estimation of daytime ecosystem respiration to determine gross primary production of a mountain meadow. Agric. For. Meteorol. 130, 13–25. https://doi.org/10.1016/j.agrformet.2005.02.001.
Wullschleger, S.D., 1993. Biochemical limitations to carbon assimilation in C_3 plants—a retrospective analysis of the A/C_i curves from 109 species. J. Exp. Bot. 44, 907–920. https://doi.org/10.1093/jxb/44.5.907.
Xue, B.-L., Kumagai, T., Iida, S., Nakai, T., Matsumoto, K., Komatsu, H., Otsuki, K., Ohta, T., 2011. Influences of canopy structure and physiological traits on flux partitioning between understory and overstory in an eastern Siberian boreal larch forest. Ecol. Model. 222, 1479–1490. https://doi.org/10.1016/j.ecolmodel.2011.01.021.
Yang, Q., Blanco, N.E., Hermida-Carrera, C., Lehotai, N., Hurry, V., Strand, Å., 2020. Two dominant boreal conifers use contrasting mechanisms to reactivate photosynthesis in the spring. Nat. Commun. 11, 128. https://doi.org/10.1038/s41467-019-13954-0.
Yin, X., Niu, Y., Putten, P.E.L.v.d., Struik, P.C., 2020. The Kok effect revisited. New Phytol. 227, 1764–1775. https://doi.org/10.1111/nph.16638.